

1 **Hierarchical porous carbon material restricted Au catalyst for highly**
2 **catalytic reduction of nitroaromatics**

3 Lei Qin ^{a,b,1}, Huan Yi ^{a,b,1}, Guangming Zeng ^{a,b,*}, Cui Lai ^{a,b,*}, Danlian Huang ^{a,b}, Piao
4 Xu ^{a,b}, Yukui Fu ^{a,b}, Jiangfan He ^{a,b}, Bisheng Li ^{a,b}, Chen Zhang ^{a,b}, Min Cheng ^{a,b}, Han
5 Wang ^{a,b}, Xigui Liu ^{a,b}

6 ^a *College of Environmental Science and Engineering, Hunan University, Changsha,*
7 *410082, PR China*

8 ^b *Key Laboratory of Environmental Biology and Pollution Control, Hunan University,*
9 *Ministry of Education, PR China*

Accepted MS

* Corresponding author at: College of Environmental Science and Engineering, Hunan University, Changsha, Hunan 410082, China. E-mail address: zgming@hnu.edu.cn (G.M. Zeng) and laicui@hnu.edu.cn (C.Lai).

¹ These authors contribute equally to this article.

10 **Abstract**

11 In this study, four kinds of porous carbon materials were used as supports to anchor
12 gold nanoparticles (AuNPs) for catalytic reduction of nitroaromatics and 4-nitrophenol
13 (4-NP) was employed as a model material. Results identified that carbon black (CB)
14 restricted-Au catalyst (Au/CB) provided large specific surface area, small AuNPs size,
15 and low cost, which showed highly catalytic activity for 4-NP reduction. Besides, with
16 the increase of Au loadings, the catalytic activity of Au/CB was enhanced and the 1.2
17 wt% of Au loading exhibited the best catalytic activity with the high rate of 0.8302 min^{-1}
18 1 and the turnover frequency of 492.50 h^{-1} . Universality and real water application
19 demonstrated that the as-prepared Au/CB catalyst was promising candidate for other
20 phenols and azo dyes reduction and had great potential for practical application.
21 Furthermore, after ten cycles, Au/CB still retained satisfying stability and activity.
22 These results suggested that the larger specific surface area and smaller particle size
23 attributing to the porosity of CB were conducive to improving the catalytic activity of
24 Au catalysts. This design shows high potential of hierarchical porous carbon materials
25 for highly catalytic reaction in many fields, especially the water purification.

26 **Keywords:** Au catalyst; carbon black; hierarchical porous carbon; nitroaromatics;
27 reduction.

28 1. Introduction

29 Nowadays, human is facing the severe threat of environmental pollution since the
30 rapid development of industrialization, especially the water pollution [1-6]. The
31 pollutants enter into plants and animals through water circulation and finally
32 accumulate in human body, which can induce serious body damage [7-11].
33 Nitroaromatics, mainly generated from industry and agriculture, are known as the
34 hazardous and toxic pollutant [12]. In particular, 4-nitrophenol (4-NP) as a kind of
35 typical nitroaromatic is considered as one of the most common pollutant in
36 environmental water and industrial wastewater [13, 14]. It is highly toxic and can result
37 in liver, kidney, central nervous system, and blood system damage [15, 16]. However,
38 these pollutants are difficult to remove because of the high structural stability. Thus, it
39 is important to develop efficient method to remove them from water.

40 As one kind of stable and non-toxic nanoparticles, gold nanoparticles (AuNPs) have
41 been widely used in many fields especially environmental protection due to its excellent
42 properties [17-21]. Particularly, the outstanding performance in catalysis of it with
43 small size has gained tremendous interests, especially in the catalytic reduction of 4-
44 NP [22, 23]. In this case, the high toxic 4-NP, one kind of "Priority Pollutant" listed by
45 the USEPA, is efficiently converted to less toxic 4-aminophenol (4-AP) under mild
46 reaction conditions, which reduces the risk of environmental pollution [24, 25]. On the
47 other hand, the product of 4-AP plays important industrial roles on the preparation of
48 drugs, dyes, corrosion inhibitors, and photographic developers, which brings huge
49 economic benefits [26]. However, colloidal AuNPs are easy to aggregate because of its
50 high surface energy and always need protective agent in the preparation process [27-
51 29]. It is obvious that the catalytic activity will be limited and the energy consumption
52 will increase. Thus, it is necessary to develop an effective way to retain the high

53 dispersity and catalytic activity of AuNPs.

54 With this respect, heterogeneous Au catalysts have been developed [30]. The
55 reusability of AuNPs has also been improved. Simultaneously, how to further enhance
56 the catalytic activity has become another topic. In this case, previous reports proposed
57 some feasible approaches: (1) decrease the particle size and narrow the size distribution
58 to improve the catalytic activity [31, 32]; (2) introduce bimetallic or multi-metallic NPs
59 to make use of the synergetic effect generated by these metals [33, 34]; (3) introduce
60 porous structure to restrict AuNPs and enhance the adsorption of 4-NP [35]. Porous
61 carbon materials are good candidates because of their excellent adsorption capacity,
62 good thermal and chemical stability, and admirable mechanical properties [36-39].
63 Among them, hierarchical porous carbon black (CB), like Vulcan XC-72, has been
64 widely used for the supports, sensors, energy storage or commercial applications due
65 to the advantages of turbostratic structures with high surface area and conductivity,
66 excellent chemical and mechanical stability [40-43]. Particularly, its properties of low
67 cost and easy availability provide an alternative for cost reduction. Besides, there are also
68 many papers have investigated the electrochemical performance of CB-supported metal
69 NPs [44]. However, to our knowledge, few of them have mentioned the catalytic
70 reduction of nitroaromatics by CB-supported catalysts in the presence of NaBH_4 .

71 It is reported that pristine CB is difficult to anchor metal ions or metal NPs because
72 of the low content of oxygen-containing groups on the surface [45, 46]. Therefore, most
73 of papers have investigated the property of modified CB via acidification or doping [47,
74 48]. Nevertheless, investigation on the performance of pristine CB as support is also
75 interesting. Because pristine CB is easy to aggregate and there are abundant pore
76 structures in CB in spite of pristine CB contains low content of oxygen-containing
77 groups, which might be beneficial to restrict the growing of AuNPs in the pore. In

78 addition, aggregated CB may provide hierarchical porous structure, including micro,
79 meso and macro pores, which result in large surface to volume ratio, reduced diffusion
80 resistance, and enhanced transport diffusion [49]. Thus, smaller AuNPs can be
81 dispersed in CB, the activity, stability and usability would be enhanced also. In addition,
82 CB can provide strong adsorption ability of CB for nitrophenols and dyes due to the π -
83 π stacking interaction and abundant pore structures. The fast electron transfer from CB
84 to AuNPs may cause higher local electron densities and hence enhance the uptake of
85 electron by nitrophenols and dyes. The catalytic activity of Au/CB may can be
86 improved either. Therefore, it is of great importance to investigate the property of
87 pristine CB as support for Au catalyst and the contribution of pore structures to that of
88 the catalytic activity.

89 In this study, CB restricted Au catalyst was prepared by a simple polyols method,
90 which using ethylene glycol (EG) as the dispersing agent of CB and reducing agent of
91 AuNPs. The reduction of 4-NP by NaBH_4 was employed as a model reaction to
92 investigate the catalytic performance of Au/CB catalyst. As comparison, three kinds of
93 typical and well-investigated porous carbon materials, including multi-walled carbon
94 nanotubes (MWCNTs), Activated Cokes (ACk), and activated carbon (AC) were used
95 to anchor AuNPs (Au/C) for the reduction of nitroaromatics. Various technologies,
96 including transmission electron microscopy (TEM), X-ray diffraction (XRD), X-ray
97 photoelectron spectroscopy (XPS), Fourier transform-infrared spectroscopy (FT-IR),
98 scanning electron microscopy (SEM), inductively coupled plasma optical emission
99 spectrometer (ICP-OES), N_2 -Brunauer-Emmett-Teller (BET), and Electron
100 paramagnetic resonance (EPR), were used to characterize the property of these catalysts
101 and to gain insight into the mechanism of the catalytic reaction. The crystalline structure
102 of the prepared Au/CB catalyst before and after reaction was characterized either. The

103 universality and real water application of as-prepared Au/CB were further proposed.

104 **2. Experimental section**

105 2.1. Preparation of carbon supported Au catalyst

106 Preparation of Au/CB catalyst was accomplished using the polyols method [50].
107 Typically, 200 mg of commercial Vulcan XC-72 CB was suspended in 80 mL of EG
108 and sonicated for 30 min. EG served as dispersant and reducing agent. Afterwards, the
109 mixture was heated up to 85 °C under regular vigorous stirring and a moderate amount
110 of HAuCl₄ solution (10 g L⁻¹) was added to achieve the required Au loading (from 0.5
111 to 2.5 wt %). The mixture was further stirred for 4 h to obtain AuNPs and then filtrated
112 and washed by water and ethanol for several times. Finally, the as prepared catalyst was
113 dried in an oven at 60 °C before use. Other carbon supported Au catalysts including
114 Au/ACk, Au/AC, and Au/MWCNTs were prepared with the same procedure.

115 2.2. Catalytic reduction performance

116 To investigate the catalytic activity of prepared Au/C catalysts, reduction of phenols
117 and azo dyes with NaBH₄ was performed. All the catalytic process were proposed as
118 the procedure of 4-NP reduction by Au/CB. Firstly, 50 mL of 4-NP (0.5 mM) was
119 freshly prepared and 10 mg of aforementioned catalyst was added under continuous
120 stirring for 1 h to achieve the adsorption-desorption equilibrium. Then, different amount
121 of NaBH₄ (the molar amount is 100, 200, 250, 300, 350, 400 times over 4-NP,
122 respectively) was added into the mixture with stirring. The catalytic progress was
123 evaluated by taking 1 mL of the reaction mixture at specified time intervals and diluted
124 five times with ultrapure water. The diluted reaction mixture was measured by UV-Vis
125 spectrometry. After reaction, the catalysts were removed by filtration and washed with
126 water and ethanol, then reused for 10 times. The catalytic performance of Au/CB on
127 real water, including bottled water, tap water, lake water, and river water (collected from

128 convenience store, our laboratory, Lake of Peach, and Hsiang River (Changsha, China),
129 respectively), was carried out. The catalytic progress was performed as the reduction of
130 4-NP in ultrapure water. All the results were achieved by three parallel experiments.

131 **3. Results and discussion**

132 3.1. Characterization of Au/CB catalyst

133 The morphology and microstructure of pure CB and Au/CB catalyst were verified by
134 the TEM characterization. As shown in **Fig. 1a-b**, CB has a typically spherical
135 morphology with the size about 30 nm and tends to aggregate because of the high
136 surface energy and van der Waal's forces [47]. The crystal plane (002) of graphite with
137 a lattice space of 0.34 nm is marked with yellow lines in **Fig. 1c**, which represents plane
138 between two single graphene layers in CB [51]. The analysis of the as-synthesized
139 Au/CB catalyst shows that AuNPs are uniformly dispersed on CB with the average size
140 of 2.5 nm (**Fig. 1d-f**). The high resolution TEM image exhibited in **Fig. 1f** clearly
141 suggests a lattice of AuNPs with a space of 0.256 nm that can be attributed to the (111)
142 plane of AuNPs, which indicates the successful deposition of AuNPs.

143 The comparison of XRD analysis for CB and Au/CB catalyst before reaction and
144 after several cycles is depicted in **Fig. 2**. It is observed that the characteristic peaks in
145 the pattern of CB at 25.0° ($d=0.36$ nm) and 43.2° ($d = 0.20$ nm) are attributed to the
146 (002) and (101) plane reflection of carbon materials. After deposition of AuNPs, the
147 well-defined diffraction peaks of Au/CB located at 38.3 , 44.4 , 64.6 , 77.6 , and 81.8° are
148 indexed to the (111), (200), (220), (311), and (222) crystal plane reflections of Au
149 (JCPDS 04-0784), respectively. However, the characteristic peak of (002) reflection is
150 broad and weak and that of (101) plane disappears. This is because the deposition of
151 AuNPs weakens the internal structure order of CB. This also proves the successful
152 deposition of AuNPs in CB. Meanwhile, after several cycles, all of the crystal plane

153 reflections of Au still exist, but the intensity of peaks has decreased. This implies there
154 may be some AuNPs losing after several reaction cycles.

155 The XPS spectra of CB, Au/CB, and Au/CB after several cycles were used to
156 determine the elemental composition and chemical state of them. As illustrated in **Fig.**
157 **3a**, the XPS survey spectra demonstrate that there were C and O as the primary elements.
158 The contents of O were very low and the Au in Au/CB before and after several cycles
159 was unobvious. While in **Fig. 3b**, the high-resolution spectra for Au 4f of them are
160 measured. The Au 4f_{7/2} and 4f_{5/2} peaks are observed at 84.7, 88.4, 84.5, and 88.2 eV of
161 Au/CB before and after several cycles respectively, which are typical values of Au in
162 zero oxidation state [52]. Besides, a new peak at 86.6 eV assigned to the Au(III)
163 oxidation state in Au/CB before catalytic reaction is observed. This may be because
164 cationic Au species were formed and stabilized on the surface of CB by hydroxyl
165 groups for the formation of Au-O interfacial bonds [53]. After reaction, the intensity of
166 Au 4f_{7/2} and 4f_{5/2} peaks are much lower than that of the one before reaction. This may
167 be because the part of AuNPs on the surface of CB were lost after several cycles. The
168 fitted C 1s spectra of them are exhibited in **Fig. 3c**. The peaks at 284.78, 285.5 and
169 290.0 eV are assigned to the sp², sp³ carbon and π-π* transition loss of CB, respectively.
170 The peaks located at 287.7 eV of CB and 287.2 eV of Au/CB are attributed to the C=O,
171 but the content is low.

172 The characteristic FT-IR spectra of CB and Au/CB catalyst with different Au
173 loadings are shown in **Fig. 3d**. They all show a series of peaks at about 1014, 2813 and
174 2887 cm⁻¹, corresponding to the stretching vibration and bending vibration of C-H from
175 the alkane group. The peaks at 1518, 1554, and 1637 cm⁻¹ are assigned to the C-C
176 stretching vibration. The rest peaks located at about 2358 and 3438 cm⁻¹ are responsible
177 for the C=C stretching vibration and O-H stretching vibration of the hydroxyl group.

178 However, although AuNPs do not show a characteristic absorption band in the FT-IR
179 spectrum, the peak of O–H stretching vibration of Au/CB is smoother than CB and
180 stronger and stronger with the increase of Au loadings, which indicates the strong
181 interaction of Au and CB [54].

182 The nitrogen adsorption-desorption isotherms and pore size distribution of CB and
183 Au/CB 1.2 wt% in the range of micropore, mesopore and macropore are showed in **Fig.**
184 **4a-b**. All apparent curves follow the typical IUPAC type IV pattern with a H₃ hysteresis,
185 suggesting the presence of mesopores and macropore. Interestingly, the BJH pore size
186 distribution further reveals that the main pore size contributions of them are macropores
187 of 108.61 and 114.38 nm (**Fig. 4b**). In addition, the micropore pore size distribution
188 suggests that there are also micropores and the main micropore size contributions are
189 0.73 and 0.75 nm for CB and Au/CB (inset of **Fig. 4b**). According to the TEM analysis,
190 the pore of dispersed CB is micropore. Hence, the mesopores and macropore in CB
191 may be because of the aggregation of dispersed CB. Interestingly, the main size
192 contribution of CB is changed from micropore to macropore after the deposition of
193 AuNPs. The calculated porous properties of CB and Au/CB with different Au loadings
194 are summarized in **Table S1**. Results indicated that there were distinct hierarchical
195 porous structures in them. Large specific surface area and hierarchical porous structure
196 were beneficial for the adsorption of organic molecules, resulting in improved catalytic
197 performance of Au/CB. Furthermore, the deposition of Au decreased the specific
198 surface area, pore volume, and average pore size, indicating the pores of CB were
199 blocked by Au. It is reasonable to suppose that AuNPs were restricted in the porous
200 channel of CB.

201 3.2. Catalysis properties of Au/CB

202 The catalytic performance of as-prepared Au/CB catalysts was explored in the

203 catalytic reduction of 4-NP by NaBH₄ as a model reaction at ambient temperature. The
204 absorption peak of 4-NP in the UV-Vis spectra located at 317 nm, and shifted at 401
205 nm in the presence of NaBH₄ (**Fig. S1**). The color also changed from light yellow to
206 bright yellow with the addition of NaBH₄ and it did not change even for a month (inset
207 of **Fig. S1**). This change is because of the formation of nitrophenolate ions in the
208 alkaline medium of NaBH₄, which confirms that the catalytic reduction was not
209 triggered when only NaBH₄ was present. However, with the addition of a small amount
210 of Au/CB (0.2 g L⁻¹), the absorption peak of 4-NP decreased and a new peak at 301 nm
211 increased subsequently. The color changed from bright yellow to colorless, suggesting
212 the production of 4-AP. During the whole reduction process, the amounts of NaBH₄
213 were much higher than that of 4-NP. Hence, the pseudo-first order kinetics can be used
214 to describe the reduction process [55]. The performance of as-prepared catalysts can be
215 evaluated by the apparent rate constants (k_{app}) according to equation 1 [56].

$$216 \quad k_{app} = -\ln(C_t/C_0)/t \quad (1)$$

217 where C₀ and C_t are the concentration of 4-NP at the initial time and different reaction
218 time (t), they can be replaced with the absorbance of 4-NP (namely A₀ and A_t). In this
219 respect, the catalytic performance of different Au loadings was investigated. The
220 corresponding k_{app} for Au/CB with different Au loadings are listed in **Table S2**.

221 It is worth noting that the calculated loadings of Au are 0.5, 1.0, 1.5, 2.0, and 2.5 wt%
222 respectively. However, the measurement contents of them by ICP-OES are 0.4, 0.88,
223 1.2, 1.34, and 1.39 wt%, which are lower than the theoretical values. One of the reason
224 may consist in the relatively low amount of oxygen-containing groups in CB, which
225 limits the ability to anchor metal NPs on the surface [42]. With the increase of Au
226 amount, the deposition sites of CB are plateaued, leading to the loss of AuNPs. Another
227 possible reason is that AuNPs are reduced partially, resulting from the loss of HAuCl₄.

228 In any case, with the increase of Au loadings, the catalytic activity of Au/CB is
229 increased. Au/CB with 1.2 wt% exhibits the highest catalytic activity with the k_{app} of
230 0.8302 min^{-1} (**Fig. 5**). As the loadings increase sequentially, the activity of Au/CB tends
231 to decrease inversely. It is possibly because larger amount of AuNPs reduced the porous
232 channel of CB, decreasing the specific surface area, pore size, and pore volume of
233 catalyst, thus limiting the adsorption of 4-NP (**Table S2**). In addition, the turnover
234 frequency (TOF) of Au/CB with different Au loadings was further calculated to
235 evaluate the catalytic efficiency of as-prepared Au/CB catalysts. As exhibited in **Table**
236 **S2**, the TOF of Au/CB with 1.2 wt% loading is much higher (49750 h^{-1}) than the others,
237 implying it exhibits better catalytic performance compared to the other loadings.
238 Besides, this work shows good catalytic performance when compared with other
239 previous reports (**Table S3**).

240 It is necessary to investigate the effect of NaBH_4 concentration because this reduction
241 reaction was triggered by NaBH_4 . To investigate the influence on catalytic performance
242 with different amounts of NaBH_4 , the molar amount of NaBH_4 for 100, 200, 250, 300,
243 350, and 400 times over 4-NP was added to trigger the catalytic reduction. As indicated
244 in **Fig. S2**, the k_{app} increased significantly with the increase of NaBH_4 . However, over
245 300 times of NaBH_4 , the rates of rise reached the maximum because the reactants were
246 saturated and the rate could not be improved even with more NaBH_4 . This phenomenon
247 is similar to the reported paper [57]. Hence, in this paper, the concentration of NaBH_4
248 was chosen as 300 times over the amount of 4-NP, namely 150 mM.

249 3.3. Catalytic performance of other Au/C catalysts

250 ACK and AC are both biomass charcoals with abundant porous structure and huge
251 specific surface area. MWCNTs are widely used in environmental remediation. In order
252 to explore the performance of porosity on Au catalysts for catalytic reduction, these

253 four kinds of porous carbon materials were employed as supports to anchor AuNPs.
254 The reduction of 4-NP by these catalysts were also proposed as comparison. The UV-
255 Vis spectra and pseudo-first-order kinetics fitting plot at suitable intervals are illustrated
256 in **Fig. 6**. With the addition of catalysts, 4-NP was reduced completely about 10, 30,
257 and 14 min for Au/MWCNTs, Au/ACk, and Au/AC respectively. As expected, the
258 catalytic activity of Au/CB is much higher than the others and the reducing rates follow
259 the order of Au/CB > Au/MWCNTs > Au/AC > Au/ACk with the values of 0.8302,
260 0.4031, 0.3067, and 0.166 min⁻¹. In this case, the XRD of Au/CB, Au/MWCNTs,
261 Au/ACk, and Au/AC was measured as comparison. As shown in **Fig. S3a**, the
262 characteristic peaks of XRD representing the (111), (200), (220), (311), and (222)
263 crystal plane reflections of Au are observed in all of these catalysts, which means
264 AuNPs were successfully deposited. The peak intensity of Au/CB is higher than the
265 others, contributing to the highest catalytic activity. Interestingly, the peak intensity of
266 Au/AC is higher than Au/MWCNTs, while the catalytic activity of Au/MWCNTs is
267 better. To explain this phenomenon, the TEM of them was further measured. As
268 obviously observed in **Fig. S3b-d**, AuNPs are successfully deposited on MWCNTs,
269 ACk, and AC, but the AuNPs in Au/AC are aggregated obviously. It is reported that the
270 catalytic activity of AuNPs were higher with the smaller particle size when the loading
271 amount was the same [58]. Thus, the aggregated AuNPs in Au/AC drastically decreased
272 the catalytic activity. Besides, the particles are well dispersed in Au/MWCNTs and the
273 size of AuNPs in it about 5 nm is much smaller than the others. Thus, it is reasonable
274 that the catalytic activity of Au/MWCNTs is higher than Au/AC and Au/ACk. Even so,
275 it is important to remark that the catalytic activity of Au/MWCNTs is still lower than
276 Au/CB because the size of AuNPs in Au/CB is smaller than Au/MWCNTs. On the other
277 hand, the BET surface area of MWCNTs is about 110 m² g⁻¹, which is much smaller

278 than CB, hence limiting the adsorption of 4-NP and further decreasing the catalytic
279 activity.

280 3.4. Test of universality, stability, and practical application

281 In order to illustrate the universality of Au/CB catalyst, the catalytic reduction of
282 other typical phenols and azo dyes, including 2-nitrophenol (2-NP), 3-nitrophenol (3-
283 NP), 2, 4-dinitrophenol (2, 4-DNP), Congo red (CR), methyl orange (MO), and
284 Erichrome Black T (EBT), by Au/CB with 1.2 wt% loading was also proposed with the
285 same procedure of 4-NP reduction. The UV-Vis spectra and pseudo-first-order kinetics
286 fitting parameters of them are provided in **Fig. 7** and **Table S4**. The results suggest that
287 these compounds can be well reduced and the catalytic rate follows the order of MO>4-
288 NP>2-NP>3-NP>2, 4-DNP>EBT>CR with catalytic rates of 1.2869, 0.8302, 0.4599,
289 0.4459, 0.4287, 0.4085, and 0.3652 min⁻¹, respectively. The results are highly
290 corresponded with the reported papers [46, 59]. It also demonstrates that this Au/CB
291 catalyst can be used widely. Interestingly, the 2, 4-DNP with NaBH₄ shows two
292 absorption peaks at about 258 and 360 nm in the UV-Vis spectrum. The two peaks at
293 258 and 360 nm decrease gradually with the addition of Au/CB and two new peaks
294 appear at 276 and 442 nm, which indicates the formation of 2, 4-dinitrophenolate
295 intermediate. With the further increasing of reaction time, the peak at 442 nm decreases
296 and a new peak at 300 nm appears. The color of 2, 4-DNP also changes from yellow to
297 pale orange and colorless during the whole reaction process. These results indicate the
298 formation of 2, 4-diaminophenol and are in well agreement with the previous reports
299 [60, 61].

300 To investigate the stability and reusability, the Au/CB was reused to reduce 4-NP
301 about 10 cycles. As exhibited in **Fig. 8**, the Au/CB shows continuous decrease of
302 catalytic activity within the first several recycles, but still reveals a high catalytic

303 efficiency of 4-NP reduction. After the third cycle, the activity of Au/CB tends to be
304 stable. It may be because the loss of AuNPs on the surface decrease the catalytic activity,
305 while the AuNPs inside remain stable catalytic activity for 4-NP reduction. Combining
306 the results of XPS and XRD for Au/CB before and after several cycles, we speculate
307 that AuNPs on the surface may be easy to loss but AuNPs restricted in the pore channels
308 are stable and can provide good catalytic activity.

309 On the other hand, the catalytic performance on real water samples is very important.
310 On this basis, reduction of 4-NP by Au/CB with 1.2 wt% loading on bottled water, tap
311 water, lake water, and river water was performed. Obviously, 4-NP can eventually be
312 completely reduced in these samples (**Fig. 9**), and the catalytic rates are 0.4480, 0.3613,
313 0.2800, and 0.1303 min⁻¹ for river water, bottled water, lake water, and tap water, in
314 which the catalytic activity on tap water is the lowest one. This is possible because there
315 are disinfectants or plenty of dissolved oxygen (DO) which can consume NaBH₄,
316 leading to limited catalytic activity. In this case, the concentration of ClO⁻, Cl⁻, and DO
317 in these samples were detected. As shown in **Table S5**, the concentrations of ClO⁻ and
318 DO in tap water are higher than the others, especially the ClO⁻ is not found except in
319 the tap water. This results verify the speculation that the catalytic activity of Au/CB in
320 real water is highly connected with the concentration of ClO⁻ and DO. However, the
321 concentration of DO in lake water is the lowest, but the activity is lower than the river
322 water. This may be because of the presence of Cl⁻ in lake water, which will poison the
323 catalyst, thus reducing the catalytic efficiency. Anyway, the results for real water
324 application reveal that the prepared Au/CB catalyst has great potential for practical
325 application.

326 3.5. Mechanistic insight in the reduction of nitroaromatics by Au/CB system

327 Dispersed CB is spherical but easy to aggregate. According to the above analysis, we

328 speculated that some CBs were aggregated, resulting in the formation of macropore and
329 mesoporous. Most of AuNPs were restricted inside the pores of CB. To verify this
330 speculation, the SEM images with EDS analysis of Au/CB catalyst were proposed. As
331 observed from **Fig. S4**, most of elements on the surface of Au/CB are C and O, while a
332 very small part is Au. In addition, Au is not even detected in some places. The low
333 content of AuNPs on the surface of Au/CB catalyst is similar with the results of XPS.
334 However, the XRD analysis showed relatively strong diffraction peaks of AuNPs in
335 Au/CB. The TEM images also demonstrated the presence of dispersed AuNPs. Hence,
336 the possible mechanism of this reaction is proposed. Due to the excess use of NaBH₄
337 and the calculation of pseudo-first order kinetics, the mechanism of this reaction can be
338 proposed as the Langmuir–Hinshelwood model. As shown in **Scheme 1**, when
339 nitroaromatics added in the system, they are rapidly adsorbed on the surface of CB
340 because of the π - π stacking interaction, which promoting the access of nitroaromatics
341 to AuNPs. In addition, the strong electron-withdrawing ability of nitro-group in
342 nitroaromatics further enhances the π - π stacking interaction between nitroaromatics and
343 CB [62]. As the presence of NaBH₄, it reacts with water and plenty of activation
344 hydrogen (i.e. H[•] radical species) is released. Subsequently, AuNPs capture the H[•]
345 radical species to form Au-H bond. Due to the electronegativity discrepancy between
346 H[•] and Au, positively charged N in the nitro-group of nitroaromatics is attacked by H[•].
347 The nitro-group is successfully reduced to nitroso group, hydroxylamine, and finally
348 turns into the corresponding products. To verify the formation of Au-H bond and
349 identify the role of AuNPs, EPR with 5, 5-Dimethylpyrroline N-oxide (DMPO) as a
350 spin trapper was proposed to explore the evolution of H[•] radical species. As shown in
351 **Fig. S5a**, a high signal intensity of nine-line SPR spectra is observed when DMPO
352 presents in the solution containing NaBH₄, 4-NP + NaBH₄, and 4-NP + NaBH₄ +

353 Au/CB 1.2 wt%. These spectra are composed by a 1:1:1 triplet of 1:2:1 triplets with a_N
354 = 16.62 G and $a_H = 22.58$ G, which means there are plenty of H^\bullet radical adducts in the
355 solutions. Simultaneously, no signal is observed in the absence of $NaBH_4$, which
356 indicates H^\bullet radical adducts are mainly produced by $NaBH_4$. Nevertheless, the intensity
357 of H^\bullet radical adducts is higher when Au/CB is added. This suggests the presence of
358 Au/CB can promote the generation of H^\bullet radical adducts and form the Au-H bond [63,
359 64]. Moreover, the evaluation of H^\bullet radical adducts with time change was also detected
360 (Fig. S5b). At the beginning of reaction, $NaBH_4$ is the main resource of H^\bullet radical
361 adducts. The intensity of H^\bullet radical adducts trends to be stable. With time changes, the
362 intensity increases and finally decreases, which indicates the consumption of H^\bullet radical
363 adducts and completion of catalytic reduction. Since the reduction takes place on the
364 active sites of AuNPs, the reduction process is a cycle of H^\bullet radical adducts trap and
365 transportation.

366 In this study, AuNPs are deposited both inside and on the surface of CB at the first
367 cycle. The high activity of Au/CB with the content of 1.2 wt% can be attributed to the
368 abundant hierarchical porous structure of CB and the synergistic effect of AuNPs and
369 CB. Firstly, CB has high specific surface area for restricting Au, which is in favor to
370 improve the stability. Secondly, the relatively small size and high dispersion of AuNPs
371 provides more active sites, leading to high catalytic activity. Thirdly, the strong
372 adsorption ability of CB towards phenols and dyes makes a higher concentration of
373 targets near to the AuNPs, resulting in highly efficient contact between the targets and
374 active sites. Most importantly, the property of CB with conductive matrix and
375 supercapacitance promotes the electron transfer from CB to AuNPs, causing higher
376 local electron densities and hence enhancing the uptake of electron by nitroaromatics.
377 Although there are small amount of oxygen-containing groups on the surface of CB,

378 part of AuNPs are still anchored on the surface. However, after several cycles, the
379 surface AuNPs tend to shed from CB and the catalytic activity decreases slightly.
380 Fortunately, there are plenty of AuNPs may be restricted inside of CB because of the
381 abundant porous structure. Therefore, the relatively stable and high activity can be
382 achieved.

383 **4. Conclusion**

384 In order to investigate the property of pristine CB as the support for heterogeneous
385 Au catalyst, an Au/CB catalyst was prepared by a simple polyols method for
386 nitroaromatics reduction. Different kinds of porous carbon materials including CB,
387 ACK, AC, and MWCNTs used as supports to anchor AuNPs were proposed as
388 comparison to explore the contribution of pore structures for the catalytic activity.
389 Results showed that Au/CB exhibited higher activity and lower cost than others. The
390 abundant hierarchical porous structures of CB provided strong adsorption ability of
391 nitroaromatics, which resulted in the high catalytic efficiency. Interestingly, the
392 aggregation of CB provided more pores, which were beneficial for the AuNPs
393 anchoring. The synergistic effect between AuNPs and CB further enhanced the catalytic
394 activity. In addition, this Au/CB catalyst showed good universality, stability, and
395 practical application. The hierarchical porous structures of CB are contributed to the
396 high stable and catalytic activity of Au/CB, and because of the low cost it can be further
397 used in environment field.

398 **Acknowledgments**

399 This study was financially supported by the Program for the National Natural Science
400 Foundation of China (51579098, 51879101, 51779090, 51709101, 51278176,

401 51408206, 51521006, 51809090, 51378190), Science and Technology Plan Project of
402 Hunan Province (2016RS3026, 2017SK2243, 2018SK20410), Hunan Provincial
403 Innovation Foundation For Postgraduate (CX2018B155), the National Program for
404 Support of Top-Notch Young Professionals of China (2014), the Program for New
405 Century Excellent Talents in University (NCET-13-0186), the Program for Changjiang
406 Scholars and Innovative Research Team in University (IRT-13R17), and the
407 Fundamental Research Funds for the Central Universities (531107050978,
408 531107051080, 531109200027). The authors would like to thank Xiaobing Zhou from
409 Shiyanjia Lab (www.shiyanjia.com) for the EPR analysis.

Accepted MS

410 **References**

411 [1] B. Li, C. Lai, G. Zeng, L. Qin, H. Yi, D. Huang, C. Zhou, X. Liu, M. Cheng, P. Xu,
412 C. Zhang, F. Huang, S. Liu, Facile Hydrothermal Synthesis of Z-Scheme
413 $\text{Bi}_2\text{Fe}_4\text{O}_9/\text{Bi}_2\text{WO}_6$ Heterojunction Photocatalyst with Enhanced Visible Light
414 Photocatalytic Activity, ACS Appl. Mater. Interfaces 10 (2018) 18824-18836.

415 [2] M. Cheng, G. Zeng, D. Huang, C. Lai, Y. Liu, C. Zhang, R. Wang, L. Qin, W. Xue,
416 B. Song, High adsorption of methylene blue by salicylic acid-methanol modified steel
417 converter slag and evaluation of its mechanism, J. Colloid Interface Sci. 515 (2018)
418 232-239.

419 [3] P. Xu, G.M. Zeng, D.L. Huang, C.L. Feng, S. He, M.H. Zhao, C. Lai, Z. Wei, C.
420 Huang, G.X. Xie, Use of iron oxide nanomaterials in wastewater treatment: a review,
421 Sci. Total Environ. 424 (2012) 1-10.

422 [4] H. Yi, M. Yan, D. Huang, G. Zeng, C. Lai, M. Li, X. Huo, L. Qin, S. Liu, X. Liu, B.
423 Li, H. Wang, M. Shen, Y. Lu, X. Guo, Synergistic effect of artificial enzyme and 2D
424 nano-structured Bi_2WO_6 for eco-friendly and efficient biomimetic photocatalysis,
425 Appl. Catal. B: Environ. 250 (2019) 52-62.

426 [5] W. Wang, P. Xu, M. Chen, G. Zeng, C. Zhang, C. Zhou, Y. Yang, D. Huang, C. Lai,
427 M. Cheng, L. Hu, W. Xiong, H. Guo, M. Zhou, Alkali Metal-Assisted Synthesis of
428 Graphite Carbon Nitride with Tunable Band-Gap for Enhanced Visible-Light-Driven
429 Photocatalytic Performance, ACS Sustain. Chem. Eng. 6 (2018) 15503-15516.

430 [6] L. Li, C. Lai, F. Huang, M. Cheng, G. Zeng, D. Huang, B. Li, S. Liu, M. Zhang, L.
431 Qin, M. Li, J. He, Y. Zhang, L. Chen, Degradation of naphthalene with magnetic bio-

432 char activate hydrogen peroxide: Synergism of bio-char and Fe–Mn binary oxides,
433 Water Res. 160 (2019) 238-248.

434 [7] C. Lai, M.-M. Wang, G.-M. Zeng, Y.-G. Liu, D.-L. Huang, C. Zhang, R.-Z. Wang,
435 P. Xu, M. Cheng, C. Huang, Synthesis of surface molecular imprinted TiO₂/graphene
436 photocatalyst and its highly efficient photocatalytic degradation of target pollutant
437 under visible light irradiation, Appl. Surf. Sci. 390 (2016) 368-376.

438 [8] X. Gong, D. Huang, Y. Liu, G. Zeng, R. Wang, J. Wan, C. Zhang, M. Cheng, X. Qin,
439 W. Xue, Stabilized Nanoscale Zerovalent Iron Mediated Cadmium Accumulation and
440 Oxidative Damage of *Boehmeria nivea* (L.) Gaudich Cultivated in Cadmium
441 Contaminated Sediments, Environ. Sci. Technol. 51 (2017) 11308-11316.

442 [9] W. Xue, D. Huang, G. Zeng, J. Wan, C. Zhang, R. Xu, M. Cheng, R. Deng,
443 Nanoscale zero-valent iron coated with rhodolipid as an effective stabilizer for
444 immobilization of Cd and Pb in river sediments, J. Hazard. Mater. 341 (2018) 381-389.

445 [10] J. Luo, T. Liu, D. Zhang, K. Yin, D. Wang, W. Zhang, C. Liu, C. Yang, Y. Wei, L.
446 Wang, The individual and Co-exposure degradation of benzophenone derivatives by
447 UV/H₂O₂ and UV/PDS in different water matrices, Water Res. 159 (2019) 102-110.

448 [11] Y. Yang, Z. Zeng, C. Zhang, D. Huang, G. Zeng, R. Xiao, C. Lai, C. Zhou, H. Guo,
449 W. Xue, Construction of iodine vacancy-rich BiOI/Ag@ AgI Z-scheme heterojunction
450 photocatalysts for visible-light-driven tetracycline degradation: transformation
451 pathways and mechanism insight, Chem. Eng. J., 349 (2018) 808-821.

452 [12] R. Abazari, A.R. Mahjoub, G. Salehi, Preparation of amine functionalized g-
453 C₃N₄@H/SMOF NCs with visible light photocatalytic characteristic for 4-nitrophenol

454 degradation from aqueous solution, *J. Hazard. Mater.* 365 (2019) 921-931.

455 [13] M. Song, Y. Wu, C. Xu, X. Wang, Y. Su, Synergistic effects of multi-active sites in
456 silver modified Bi⁰-BiVO₄ toward efficient reduction of aromatic nitrobenzene, *J.*
457 *Hazard. Mater.* 368 (2019) 530-540.

458 [14] X. Guo, Z. Peng, D. Huang, P. Xu, G. Zeng, S. Zhou, X. Gong, M. Cheng, R. Deng,
459 H. Yi, H. Luo, X. Yan, T. Li, Biotransformation of cadmium-sulfamethazine combined
460 pollutant in aqueous environments: *Phanerochaete chrysosporium* bring cautious
461 optimism, *Chem. Eng. J.* 347 (2018) 74-83.

462 [15] H. Abdullah, N. Susanto Gultom, D.-H. Kuo, Synthesis and characterization of La-
463 doped Zn(O,S) photocatalyst for green chemical detoxification of 4-nitrophenol, *J.*
464 *Hazard. Mater.* 363 (2019) 109-118.

465 [16] Z. Hu, J. Zhou, Y. Ai, L. Liu, L. Qi, R. Jiang, H. Bao, J. Wang, J. Hu, H.-b. Sun,
466 Q. Liang, Two dimensional Rh/Fe₃O₄/g-C₃N₄-N enabled hydrazine mediated catalytic
467 transfer hydrogenation of nitroaromatics: A predictable catalyst model with adjoining
468 Rh, *J. Catal.* 368 (2018) 20-30.

469 [17] R. Ciriminna, E. Falletta, C. Della Pina, J.H. Teles, M. Pagliaro, Industrial
470 Applications of Gold Catalysis, *Angew. Chem. Int. Ed.* 55 (2016) 14210-14217.

471 [18] X. Liu, D. Huang, C. Lai, G. Zeng, L. Qin, C. Zhang, H. Yi, B. Li, R. Deng, S. Liu,
472 Y. Zhang, Recent advances in sensors for tetracycline antibiotics and their applications,
473 *TrAC, Trends Anal. Chem.* 109 (2018) 260-274.

474 [19] L. Qin, G. Zeng, C. Lai, D. Huang, C. Zhang, P. Xu, T. Hu, X. Liu, M. Cheng, Y.
475 Liu, A visual application of gold nanoparticles: Simple, reliable and sensitive detection

476 of kanamycin based on hydrogen-bonding recognition, *Sens. Actuators, B* 243 (2017)
477 946-954.

478 [20] M.S. Scurrall, Thoughts on the use of gold-based catalysts in environmental
479 protection catalysis, *Gold Bull.* 50 (2017) 1-8.

480 [21] Y. Ai, Z. Hu, L. Liu, J. Zhou, Y. Long, J. Li, M. Ding, H.-B. Sun, Q. Liang,
481 Magnetically Hollow Pt Nanocages with Ultrathin Walls as a Highly Integrated
482 Nanoreactor for Catalytic Transfer Hydrogenation Reaction, *Adv. Sci.* 6 (2019)
483 1802132-1802142.

484 [22] Y. Fu, T. Huang, B. Jia, J. Zhu, X. Wang, Reduction of nitrophenols to
485 aminophenols under concerted catalysis by Au/gC₃N₄ contact system, *Appl. Catal. B:
486 Environ.* 202 (2017) 430-437.

487 [23] J.-G. You, C. Shanmugam, Y.-W. Liu, S.-J. Yu, W.-L. Tseng, Boosting catalytic
488 activity of metal nanoparticles for 4-nitrophenol reduction: Modification of metal
489 nanoparticles with poly(diallyldimethylammonium chloride), *J. Hazard. Mater.* 324
490 (2017) 420-427.

491 [24] H.G. Soğukömeroğulları, Y. Karataş, M. Celebi, M. Gülcan, M. Sönmez, M.
492 Zahmakiran, Palladium nanoparticles decorated on amine functionalized graphene
493 nanosheets as excellent nanocatalyst for the hydrogenation of nitrophenols to
494 aminophenol counterparts, *J. Hazard. Mater.* 369 (2019) 96-107.

495 [25] Y. Fu, L. Qin, D. Huang, G. Zeng, C. Lai, B. Li, J. He, H. Yi, M. Zhang, M. Cheng,
496 X. Wen, Chitosan functionalized activated coke for Au nanoparticles anchoring: Green
497 synthesis and catalytic activities in hydrogenation of nitrophenols and azo dyes, *Appl.*

498 Catal. B: Environ. 255 (2019) 117740.

499 [26] X. Zhou, C. Lai, D. Huang, G. Zeng, L. Chen, L. Qin, P. Xu, M. Cheng, C. Huang,
500 C. Zhang, C. Zhou, Preparation of water-compatible molecularly imprinted thiol-
501 functionalized activated titanium dioxide: Selective adsorption and efficient
502 photodegradation of 2, 4-dinitrophenol in aqueous solution, J. Hazard. Mater. 346 (2018)
503 113-123.

504 [27] C. Lai, X. Liu, L. Qin, C. Zhang, G. Zeng, D. Huang, M. Cheng, P. Xu, H. Yi, D.
505 Huang, Chitosan-wrapped gold nanoparticles for hydrogen-bonding recognition and
506 colorimetric determination of the antibiotic kanamycin, Microchim. Acta 184 (2017)
507 2097-2105.

508 [28] X.-Q. Qiao, Z.-W. Zhang, F.-Y. Tian, D.-F. Zhou, Z.-F. Tian, D.-S. Li, Q. Zhang,
509 Enhanced Catalytic Reduction of p-Nitrophenol on Ultrathin MoS₂ Nanosheets
510 Decorated with Noble Metal Nanoparticles, Cryst. Growth Des. 17 (2017) 3538-3547.

511 [29] C. Lai, Q. Lei, Z. Guangming, L. Yunguo, H. Danlian, Z. Chen, X. Piao, C. Min,
512 Q. Xiangbin, W. Fanmen, Sensitive and selective detection of mercury ions based on
513 papain and 2,6-pyridinedicarboxylic acid functionalized gold nanoparticles, Rsc Adv.
514 6 (2015) 3259-3266.

515 [30] A. Cho, Connecting the dots to custom catalysts, Science 299 (2003) 1684-1685.

516 [31] D.H. Barrett, M.S. Scurrall, C.B. Rodella, B. Diaz, D.G. Billing, P.J. Franklyn,
517 Achieving nano-gold stability through rational design, Chem. Sci. 7 (2016) 6815-6823.

518 [32] M. Guo, J. He, Y. Li, S. Ma, X. Sun, One-step synthesis of hollow porous gold
519 nanoparticles with tunable particle size for the reduction of 4-nitrophenol, J. Hazard.

520 Mater. 310 (2016) 89-97.

521 [33] P. Song, L.-L. He, A.-J. Wang, L.-P. Mei, S.-X. Zhong, J.-R. Chen, J.-J. Feng,
522 Surfactant-free synthesis of reduced graphene oxide supported porous PtAu alloyed
523 nanoflowers with improved catalytic activity, J. Mater. Chem., A 3 (2015) 5321-5327.

524 [34] Q. Xiao, S. Sarina, E.R. Waclawik, J. Jia, J. Chang, J.D. Riches, H. Wu, Z. Zheng,
525 H. Zhu, Alloying Gold with Copper Makes for a Highly Selective Visible-Light
526 Photocatalyst for the Reduction of Nitroaromatics to Anilines, ACS Cat. 6 (2016) 1744-
527 1753.

528 [35] A. Sahoo, S.K. Tripathy, N. Dehury, S. Patra, A porous trimetallic Au@Pd@Ru
529 nanoparticle system: synthesis, characterisation and efficient dye degradation and
530 removal, J. Mater. Chem., A 3 (2015) 19376-19382.

531 [36] D. Huang, R. Deng, J. Wan, G. Zeng, W. Xue, X. Wen, C. Zhou, L. Hu, X. Liu, P.
532 Xu, Remediation of lead-contaminated sediment by biochar-supported nano-
533 chlorapatite: accompanied with the change of available phosphorus and organic matters,
534 J. Hazard. Mater. 348 (2018) 109-116.

535 [37] W. Xiong, Z. Zeng, G. Zeng, Z. Yang, R. Xiao, X. Li, J. Cao, C. Zhou, H. Chen,
536 M. Jia, Y. Yang, W. Wang, X. Tang, Metal-organic frameworks derived magnetic
537 carbon- α Fe/Fe₃C composites as a highly effective adsorbent for tetracycline removal
538 from aqueous solution, Chem. Eng. J. 374 (2019) 91-99.

539 [38] C. Lai, S. Liu, C. Zhang, G. Zeng, D. Huang, L. Qin, X. Liu, H. Yi, R. Wang, F.
540 Huang, B. Li, T. Hu, Electrochemical Aptasensor Based on Sulfur–Nitrogen Codoped
541 Ordered Mesoporous Carbon and Thymine–Hg²⁺–Thymine Mismatch Structure for

542 Hg²⁺ Detection, ACS Sensors 3 (2018) 2566-2573.

543 [39] C. Zhou, P. Xu, C. Lai, C. Zhang, G. Zeng, D. Huang, M. Cheng, L. Hu, W. Xiong,
544 X. Wen, L. Qin, J. Yuan, W. Wang, Rational design of graphitic carbon nitride
545 copolymers by molecular doping for visible-light-driven degradation of aqueous
546 sulfamethazine and hydrogen evolution, Chem. Eng. J. 359 (2019) 186-196.

547 [40] Y. Zeng, H. Xu, D.D. Do, D. Nicholson, Adsorption of argon on graphitized carbon
548 black preloaded with methanol, ammonia and water: The role of adsorption regions and
549 adsorbates, Chem. Eng. J. 334 (2018) 1316-1327.

550 [41] Z. Chen, H. Dong, H. Yu, H. Yu, In-situ electrochemical fuel gas desulfurization
551 via carbon black-based gas diffusion electrodes: Performance, kinetics and mechanism,
552 Chem. Eng. J. 307 (2017) 553-561.

553 [42] F. Ali, S.B. Khan, T. Kamal, Y. Anwar, K.A. Alamry, A.M. Asiri, Bactericidal and
554 catalytic performance of green nanocomposite based-on chitosan/carbon black fiber
555 supported monometallic and bimetallic nanoparticles, Chemosphere 188 (2017) 588-
556 598.

557 [43] C. Zhang, W. Wang, A. Duan, G. Zeng, D. Huang, C. Lai, X. Tan, M. Cheng, R.
558 Wang, C. Zhou, W. Xiong, Y. Yang, Adsorption behavior of engineered carbons and
559 carbon nanomaterials for metal endocrine disruptors: Experiments and theoretical
560 calculation, Chemosphere 222 (2019) 184-194.

561 [44] R.M.A. Hameed, R.M. El-Sherif, Microwave irradiated nickel nanoparticles on
562 Vulcan XC-72R carbon black for methanol oxidation reaction in KOH solution, Appl.
563 Catal. B: Environ. 162 (2015) 217-226.

564 [45] J. Xia, L. Zhang, Y. Fu, G. He, X. Sun, X. Wang, Nitrogen-doped carbon black
565 supported NiCo₂S₄ catalyst for hydrogenation of nitrophenols under mild conditions, J.
566 Mat. Sci. 53 (2018) 4467-4481.

567 [46] J. Xia, G. He, L. Zhang, X. Sun, X. Wang, Hydrogenation of nitrophenols catalyzed
568 by carbon black-supported nickel nanoparticles under mild conditions, Appl. Catal. B:
569 Environ. 180 (2016) 408-415.

570 [47] Y. Hou, T. Zhao, Y. Shi, J. Fan, R. Zheng, Y. Zhang, Q. Gu, Surface modification
571 of carbon black to facilitate suspension polymerization of styrene and carbon black, J.
572 Appl. Polym. Sci., 135 (2018) 46387.

573 [48] X. Zhao, J. Zhu, L. Liang, C. Li, C. Liu, J. Liao, Wei, Biomass-derived N-doped
574 carbon and its application in electrocatalysis, Appl. Catal. B: Environ. 154-155 (2014)
575 177-182.

576 [49] S.W.L. Ng, G. Yilmaz, W.L. Ng, G.W. Ho, One-step activation towards
577 spontaneous etching of hollow and hierarchical porous carbon nanospheres for
578 enhanced pollutant adsorption and energy storage, Appl. Catal. B: Environ. 220 (2018)
579 533-541.

580 [50] S. Navalon, D. Sempere, M. Alvaro, H. Garcia, Influence of Hydrogen Annealing
581 on the Photocatalytic Activity of Diamond-Supported Gold Catalysts, ACS Appl. Mater.
582 Interfaces 5 (2013) 7160-7169.

583 [51] M. Bagavathi, A. Ramar, R. Saraswathi, Fe₃O₄ –carbon black nanocomposite as a
584 highly efficient counter electrode material for dye-sensitized solar cell, Ceram. Int. 42
585 (2016) 13190-13198.

586 [52] Y. Fu, P. Xu, D. Huang, G. Zeng, C. Lai, L. Qin, B. Li, J. He, H. Yi, M. Cheng, C.
587 Zhang, Au nanoparticles decorated on activated coke via a facile preparation for
588 efficient catalytic reduction of nitrophenols and azo dyes, *Appl. Surf. Sci.* 473 (2019)
589 578-588.

590 [53] J. Zhao, B. Wang, Y. Yue, S. Di, Y. Zhai, H. He, G. Sheng, H. Lai, Y. Zhu, L. Guo,
591 X. Li, Towards a greener approach for the preparation of highly active gold/carbon
592 catalyst for the hydrochlorination of ethyne, *J. Catal.* 365 (2018) 153-162.

593 [54] S. Lu, H. Wang, J. Zhou, X. Wu, W. Qin, Atomic layer deposition of ZnO on carbon
594 black as nanostructured anode materials for high-performance lithium-ion batteries,
595 *Nanoscale* 9 (2017) 1184-1192.

596 [55] L. Qin, G. Zeng, C. Lai, D. Huang, C. Zhang, M. Cheng, H. Yi, X. Liu, C. Zhou,
597 W. Xiong, F. Huang, W. Cao, Synthetic strategies and application of gold-based
598 nanocatalysts for nitroaromatics reduction, *Sci. Total Environ.* 652 (2019) 93-116.

599 [56] Y. Que, C. Feng, S. Zhang, X. Huang, Stability and catalytic activity of PEG-b-
600 PS-capped gold nanoparticles: a matter of PS chain length, *J. Phys. Chem., C* 119 (2015)
601 1960-1970.

602 [57] V.K. Gupta, N. Atar, M.L. Yola, Z. Üstündağ, L. Uzun, A novel magnetic Fe@Au
603 core-shell nanoparticles anchored graphene oxide recyclable nanocatalyst for the
604 reduction of nitrophenol compounds, *Water Res.* 48 (2014) 210-217.

605 [58] S. Panigrahi, S. Basu, S. Praharaj, S. Pande, S. Jana, A. Pal, S.K. Ghosh, T. Pal,
606 Synthesis and size-selective catalysis by supported gold nanoparticles: study on
607 heterogeneous and homogeneous catalytic process, *J. Phys. Chem., C* 111 (2007) 4596-

608 4605.

609 [59] L. Qin, D. Huang, P. Xu, G. Zeng, C. Lai, Y. Fu, H. Yi, B. Li, C. Zhang, M. Cheng,
610 C. Zhou, X. Wen, In-situ deposition of gold nanoparticles onto polydopamine-
611 decorated g-C₃N₄ for highly efficient reduction of nitroaromatics in environmental
612 water purification, *J. Colloid Interface Sci.* 534 (2019) 357-369.

613 [60] K. Gerelbaatar, A. Tsogoo, R. Dashzeveg, N. Tsedev, E.O. Ganbold, Reduction of
614 2,4-Dinitrophenol to 2,4-Diaminophenol Using AuNPs and AgNPs as Catalyst, *Solid*
615 *State Phenom.* 271 (2018) 76-84.

616 [61] K. Karakas, A. Celebioglu, M. Celebi, T. Uyar, M. Zuhmakiran, Nickel
617 nanoparticles decorated on electrospun polycaprolactone/chitosan nanofibers as
618 flexible, highly active and reusable nanocatalyst in the reduction of nitrophenols under
619 mild conditions, *Appl. Catal. B: Environ.* 203 (2017) 549-562.

620 [62] Q.S. Liu, T. Zheng, P. Wang, J.P. Fang, N. Li, Adsorption isotherm, kinetic and
621 mechanism studies of some substituted phenols on activated carbon fibers, *Chem. Eng.*
622 *J.* 157 (2010) 348-356.

623 [63] A. Abad, P. Conception, A. Corma, H. Garc á, Gold-organic-inorganic
624 highsurface-area materials as precursors of highly active catalysts, *Angew. Chem.* 117
625 (2005) 4134-4137.

626 [64] T.B. Nguyen, C.P. Huang, R.-a. Doong, Enhanced catalytic reduction of
627 nitrophenols by sodium borohydride over highly recyclable Au@graphitic carbon
628 nitride nanocomposites, *Appl. Catal. B: Environ.* 240 (2019) 337-347.

629

630 **Figure captions:**

631 **Fig.1.** TEM and HRTEM images of CB (a-c) and Au/CB catalyst (d-f).

632 **Fig. 2.** XRD plots of CB, Au/CB 1.2 wt% catalyst before and after catalytic reduction
633 reaction.

634 **Fig. 3.** XPS survey spectra (a), high-resolution spectra for Au 4f (b), and C 1s (c) of
635 CB, Au/CB 1.2 wt% before catalytic reduction reaction and after several cycles. (d)
636 Characteristic FT-IR spectra of CB (inset a) and Au/CB catalyst with different Au
637 loadings (0.4, 0.88, 1.20, 1.34, and 1.39 wt% inset b-f).

638 **Fig. 4.** Nitrogen adsorption-desorption isotherms (a), BJH pore size distribution (b), and
639 micropore pore size distribution (inset of b) of CB and Au/CB 1.2 wt% catalyst.

640 **Fig. 5.** Time-dependent UV-Vis absorption spectra of 4-NP catalyzed by Au/CB 1.20
641 wt% catalyst (a). Plots of $\ln(C_t/C_0)$ versus reaction time and pseudo-first-order kinetics
642 fitting of Au/CB with different Au catalysts (b).

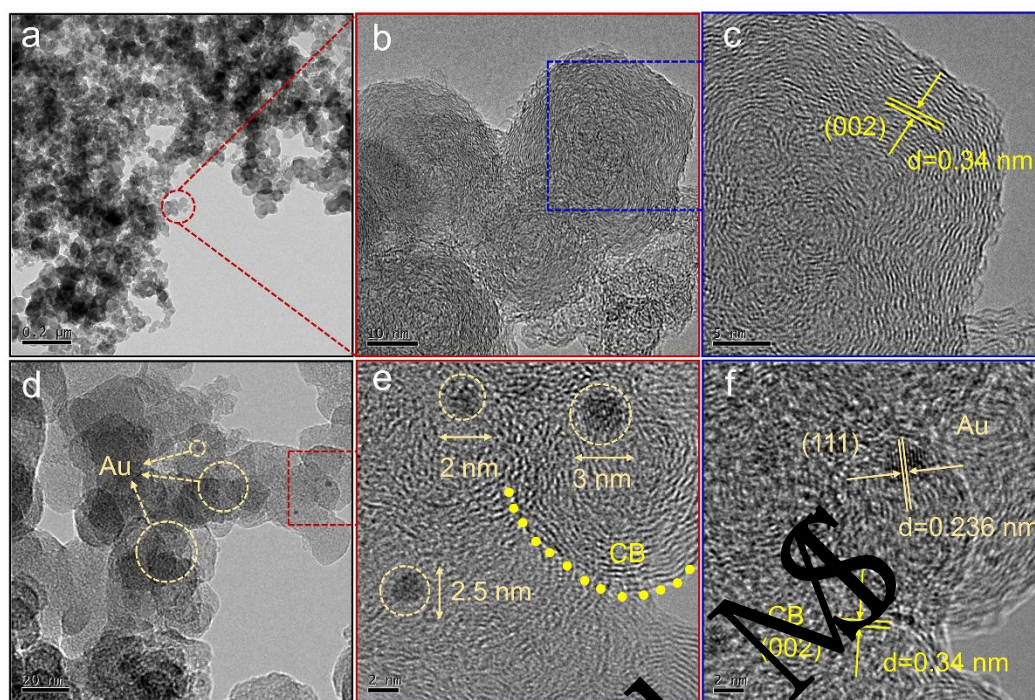
643 **Fig. 6.** Time-dependent UV-Vis absorption spectra of 4-NP catalyzed by Au/MWCNTs
644 (a), Au/ACk (b), and Au/AC (c). Plots of pseudo-first-order kinetics fitting by
645 Au/MWCNTs, Au/ACk, Au/AC, and Au/CB (d).

646 **Fig. 7.** Time-dependent UV-Vis absorption spectra of 2-NP, 3-NP, 2, 4-DNP, CR, EBT,
647 and MO reduced by Au/CB catalyst.

648 **Fig. 8.** Reusability of 4-NP reduction by Au/CB for 50 min over 10 cycles.

649 **Fig. 9.** Time-dependent UV-Vis absorption spectra of 4-NP reduction by Au/CB on
650 bottled water (a), tap water (b), lake water (c), and river water (d) and the pseudo-first-
651 order kinetics fitting plots of them (e).

652 **Scheme 1.** Mechanism of catalytic reduction of 4-NP by Au/CB catalyst before reaction
653 and after several cycles.

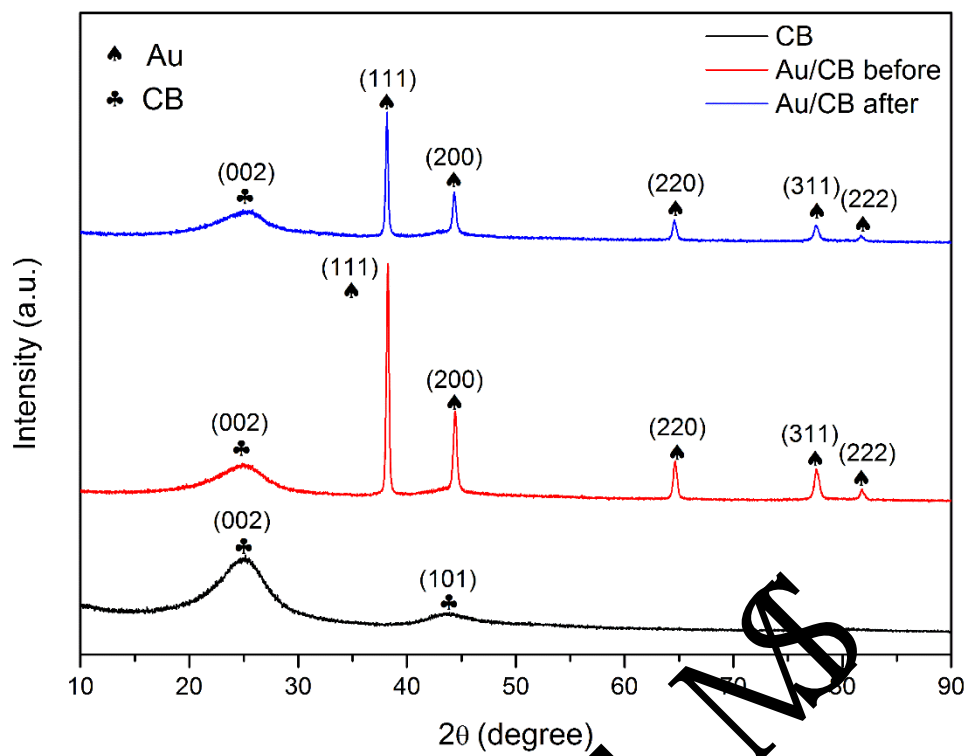


655

656 **Fig.1.** TEM and HRTEM images of CB (a-c) and Au/CB catalyst (d-f).

657

Accepted MS



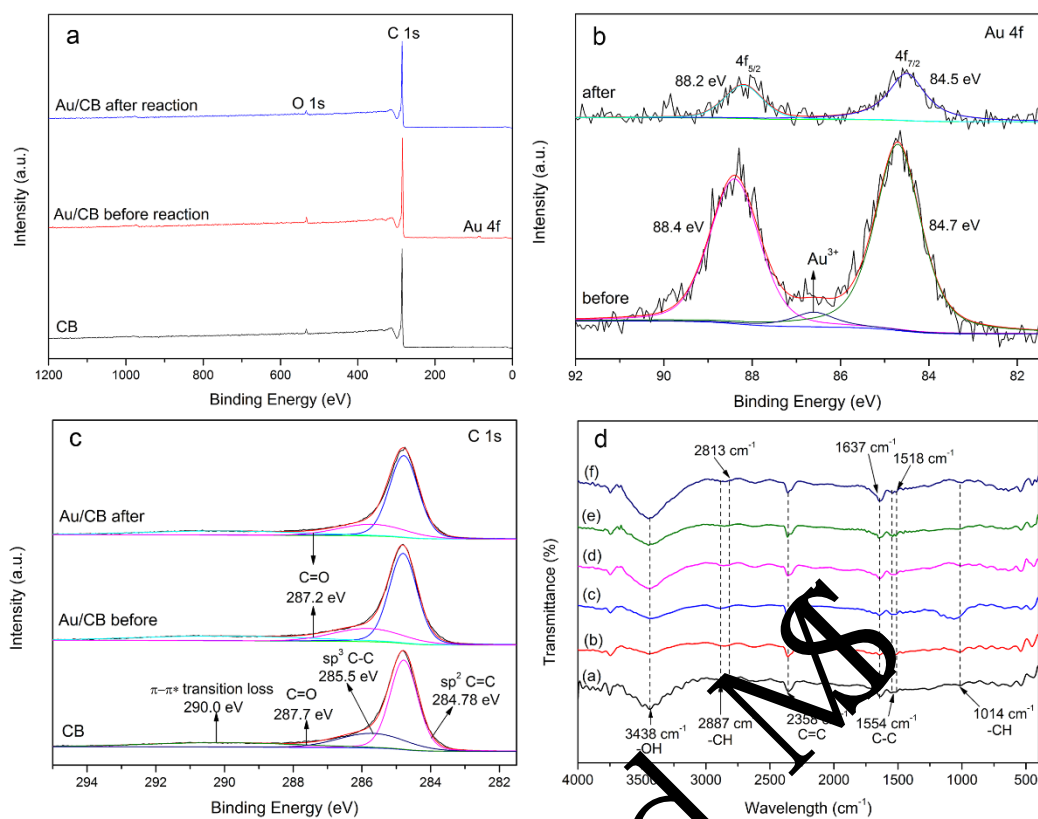
658

659 **Fig. 2.** XRD plots of CB, Au/CB 1.2 wt% catalyst before and after catalytic reduction

660 reaction.

661

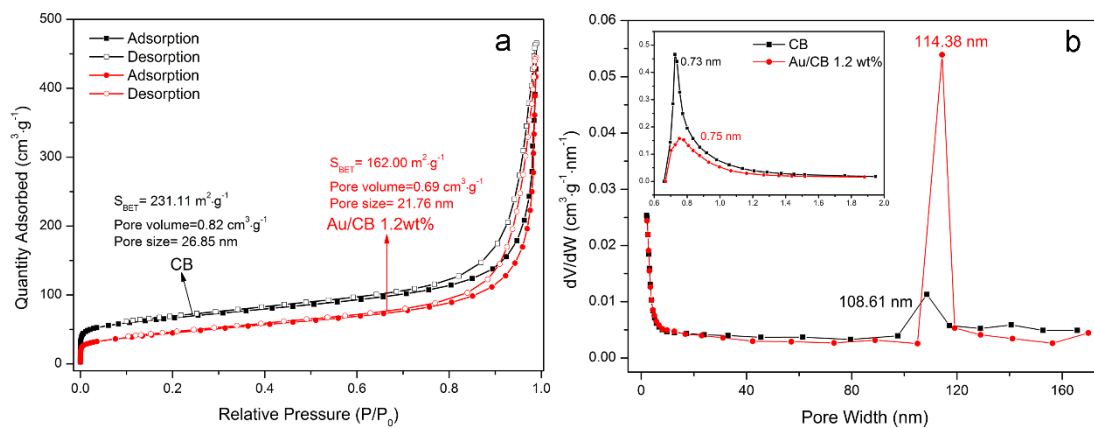
Accepted MS



662

663 **Fig. 3.** XPS survey spectra (a), high-resolution spectra for Au 4f (b), and C 1s (c) of
 664 CB, Au/CB 1.2 wt% before catalytic reduction reaction and after several cycles. (d)
 665 Characteristic FT-IR spectra of CB (inset a) and Au/CB catalyst with different Au
 666 loadings (0.4, 0.88, 1.20, 1.34, and 1.79 wt% inset b-f).

667



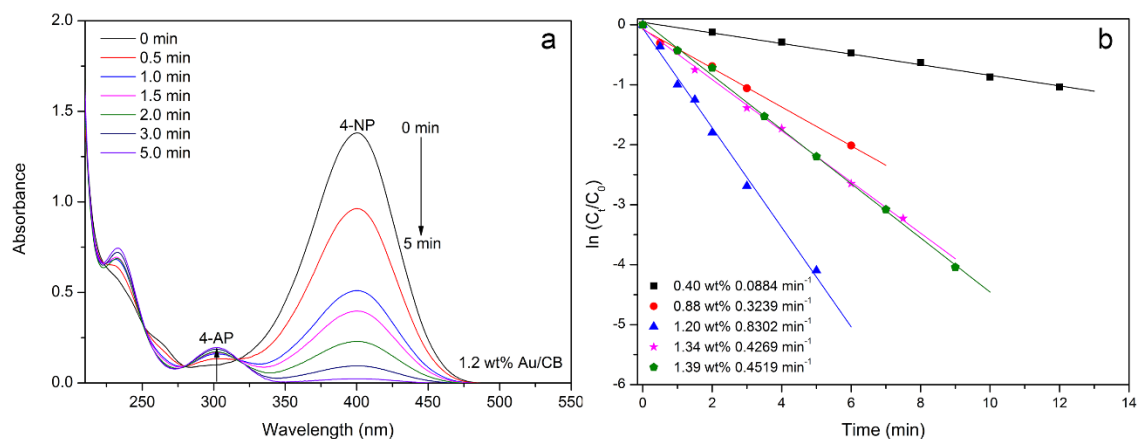
668

669 **Fig. 4.** Nitrogen adsorption-desorption isotherms (a), BJH pore size distribution (b), and

670 micropore pore size distribution (inset of b) of CB and Au/CB 1.2 wt% catalyst.

671

Accepted MS



672

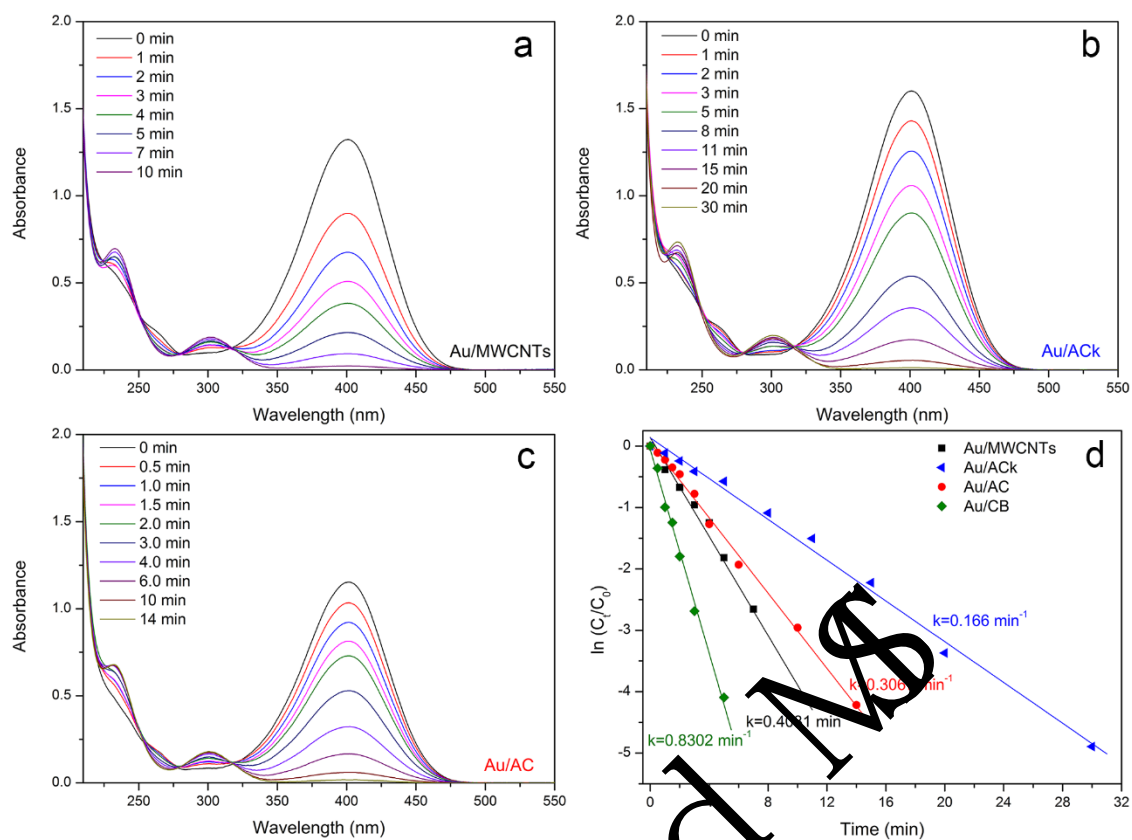
673 **Fig. 5.** Time-dependent UV-Vis absorption spectra of 4-NP catalyzed by Au/CB 1.20

674 wt% catalyst (a). Plots of $\ln(C_t/C_0)$ versus reaction time and pseudo-first-order kinetics

675 fitting of Au/CB with different Au catalysts (b).

676

Accepted MS

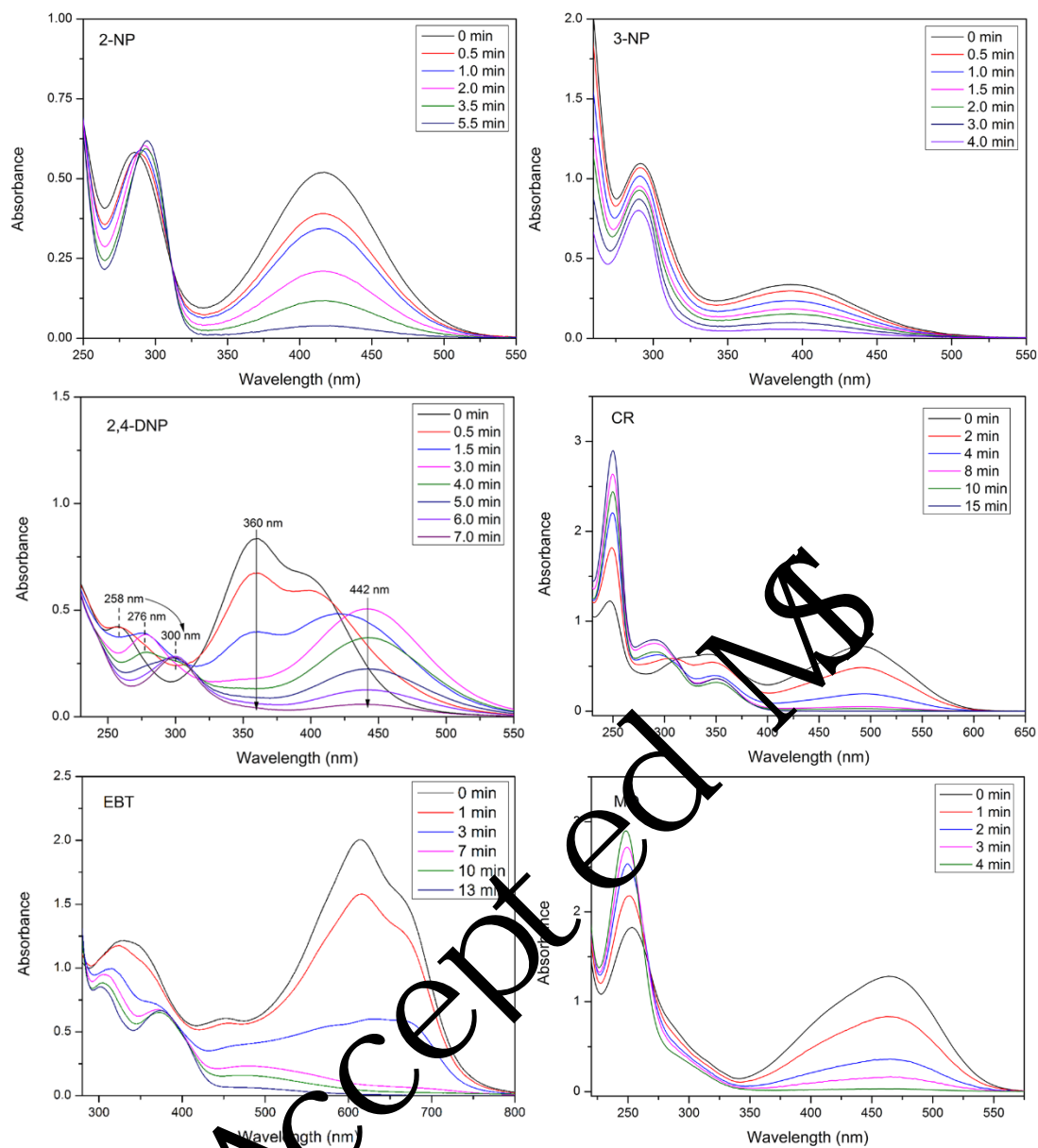


677

678 **Fig. 6.** Time-dependent UV-Vis absorption spectra of 4-NP catalyzed by Au/MWCNTs

679 (a), Au/ACK (b), and Au/AC (c). Plots of pseudo-first-order kinetics fitting by

680 Au/MWCNTs, Au/ACK, Au/AC, and Au/CB (d).

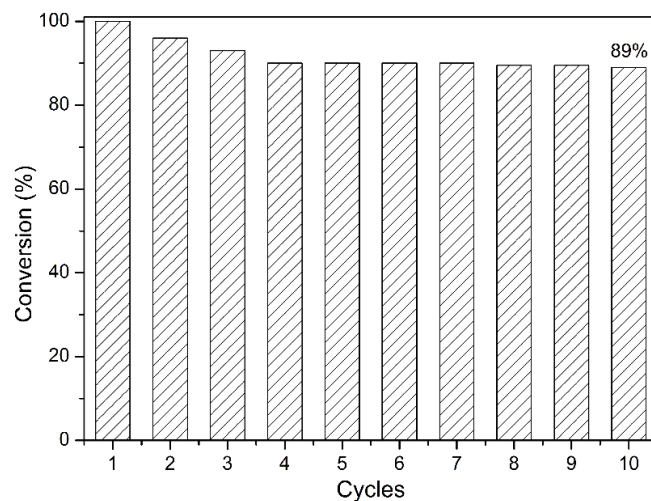


681

682 **Fig. 7.** Time-dependent UV-Vis absorption spectra of 2-NP, 3-NP, 2, 4-DNP, CR, EBT,

683 and MO reduced by Au/CB catalyst.

684

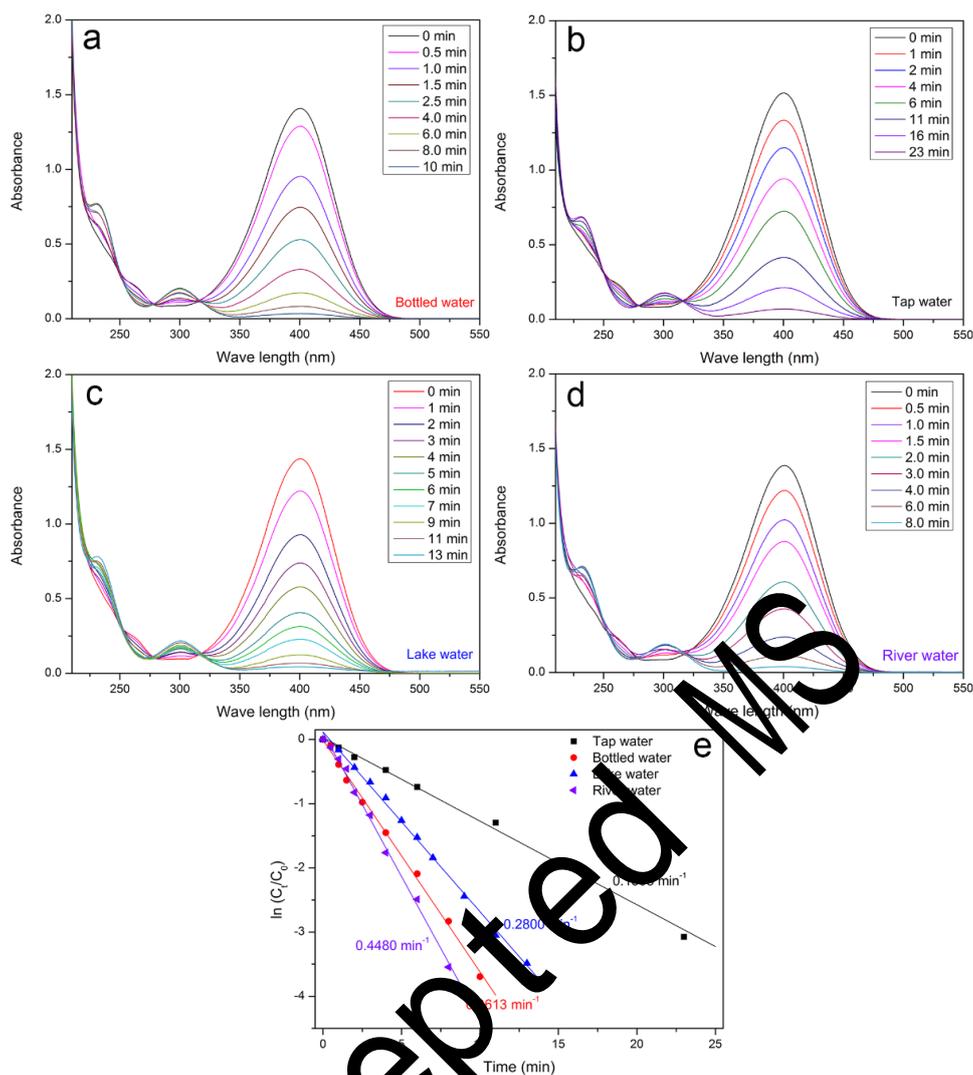


685

686 **Fig. 8.** Reusability of 4-NP reduction by Au/CB for 50 min over 10 cycles.

687

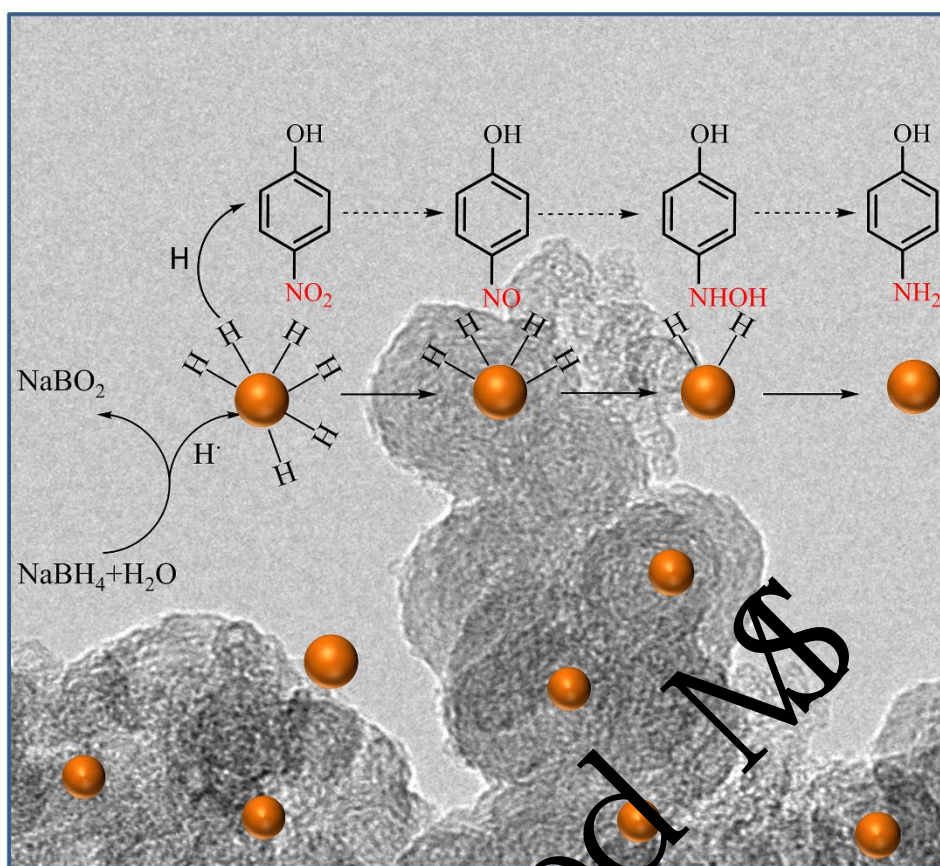
Accepted MS



688

689 **Fig. 9.** Time-dependent UV-Vis absorption spectra of 4-NP reduction by Au/CB on
 690 bottled water (a), tap water (b), lake water (c), and river water (d) and the pseudo-first-
 691 order kinetics fitting plots of them (e).

692



693

694 **Scheme 1.** Mechanism of catalytic reduction of 4-NP by Au/CB catalyst.

695

Accepted MS